ARTICLE

Photopatternable Source/Drain Electrodes using Multiwalled Carbon Nanotube/Polymer Nanocomposites for Organic Field-Effect Transistors

Kipyo Hong, Chanwoo Yang, Se Hyun Kim, Jaeyoung Jang, Sooji Nam, and Chan Eon Park*

Polymer Research Institute, Department of Chemical Engineering, Pohang University of Science and Technology, Pohang 790-784, Korea

ABSTRACT We fabricated photopatternable and conductive polymer/multiwalled carbon nanotube (MWNT) composites by dispersing MWNTs with poly(4-styrenesulfonic acid) (PSS) and poly(acrylic acid) (PAA) in water. PAA enables photo-cross-linking in the composite by adding ammonium dichromate, and PSS assists the dispersion of MWNTs in the composites, leading to higher conductivity. Composite films of PAA/PSS-MWNTs were characterized by conductivities of 1.4−210 S/cm and a work function of 4.46 eV, which could be increased to 4.76 eV during UV photo-cross-linking. By using PAA/PSS-MWNT composites as source/drain electrodes, 6,13-bis(triisopropylsilylethynyl)pentacene field-effect transistors (FET) exhibited a field-effect mobility of 0.101 ± 0.034 $cm^2/(V\ s)$, which is 9 times higher than that of FETs fabricated with gold as source/drain electrodes (0.012 ± 0.003 $cm^2/(V\ s)$).

KEYWORDS: multiwalled carbon nanotube • organic field effect transistor • photopatternable • nanocomposite electrode

1. INTRODUCTION

Organic field-effect transistors (OFETs) have considerable potential for use in cheap disposable electronic products such as radio frequency identification tags (1−3). To realize this potential, the organic materials must be processable in solution and at low temperatures. Intensive studies performed on solution-processable organic semiconductors composed of small molecules and polymers, such as 6,13-bis(triisopropylsilylethynyl)pentacene (TIPS-PEN), poly(3-hexylthiophene), and poly(2,5-bis(3-alkylthiophen-2-yl)thieno[3,2-*b*]thiophene) (4−6) have made it possible to achieve device performance comparable to that of amorphous-silicon transistors.

Source/drain electrodes used in such OFETs should also have high work functions (for p-type transistors) and high conductivities. To date, many materials, including conductive polymers, silver paste, polymer/carbon nanotube composites, and graphene (7−13), have been tested as possible electrodes for OFETs. Source/drain patterns are formed by a variety of techniques, such as inkjet printing, contact printing, imprinting, screen printing, spray printing, and selective organization techniques (7, 8, 10, 12, 14−18). Inexpensive OFET fabrication is necessary for realizing low-cost organic devices. Toward this end, printing methods are more advantageous than conventional photolithography, because photolithography generally requires several steps accompanied with using the photoresist, leading to a high process cost. When the materials used as source/drain electrodes are photo-cross-linkable, photolithography can still be used for low-cost OTFTs by removing many of the steps. However, only a few materials, such as poly(3,4-ethylenedioxythiophene):poly(styrene sulfonate) (PEDOT:PSS) with bis(fluorinated phenyl azide) (or 4,4′-diazido-2,2′-disulfonic acid benzalacetone disodium salt) and silver pastes composed of a photoactive polymer (19−22), were tested as electrodes. However, PEDOT:PSS suffers from low conductivity and silver pastes are characterized by a low work function.

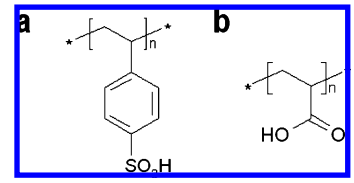

FIGURE 1. Molecular structures of (a) poly(4-styrenesulfonic acid) and (b) poly(acrylic acid).

Multiwalled carbon nanotubes (MWNTs) consist of coaxially arranged single-walled carbon nanotubes of different radii and are good candidates for use as electrodes in flexible organic devices because of their high conductivity and mechanical strength (23, 24). However, poor solubility and low work functions have limited their use. It has been reported that carbon nanotubes are solubilized in water by using polyelectrolytes such as poly(acrylic acid) (PAA) (Figure 1a), poly(4-styrenesulfonic acid) (PSS) (Figure 1b), and poly(allylamine) (25−27).

In this work, we fabricated photopatternable and conductive MWNT composites by introducing both PAA and PSS. PAA is known to be photo-cross-linkable by the addition of

* To whom correspondence should be addressed. Tel: +82-54-279-2269. Fax: +82-54-279-8298, E-mail: cep@postech.ac.kr.
Received for review July 21, 2009 and accepted October 4, 2009

DOI: 10.1021/am900483y

Published on Web 10/12/2009

ammonium dichromate (ADC) (28). However, PAA slightly ionizes in water to yield random coils that disperse the MWNTs by adsorbing to the MWNT surfaces. Therefore, PAA cannot effectively break the bundles of MWNTs. Thus, the PAA-MWNT solution consists of dispersed aggregates of large bundles of MWNTs and highly entangled nanotubes, leading to a low resolution for composite patterning. In contrast, PSS is a stronger polymer surfactant than PAA and disperses MWNTs in water by wrapping them with PSS, resulting in fewer aggregates or entangled tubes. Thus, by using both PAA as a photo cross-linkable polyelectrolyte and PSS as a strong dispersant, we fabricated MWNT composites that are photopatternable and sufficiently conductive to be used in OFETs.

2. EXPERIMENTAL SECTION

The MWNTs were purchased from Carbon Nanomaterial Technology Co. (Korea) and used as received. PSS (MW ≈ 75 000) and PAA (MW ≈ 100 000) were obtained from Aldrich. Solutions of 3 wt % PSS-MWNT, PAA-MWNTs, and PAA/PSS-MWNTs were made by dispersing nanotubes in PSS, PAA, and PAA/PSS aqueous solutions, respectively, submitting the solutions to ultrasound irradiation for 30 min with a high-intensity ultrasonic probe (Ulsso Hitech Co. (Korea), Ti-Horn, 19.87 kHz, 700 W), followed by incubation at 60 °C for 12 h. The homogeneous dispersion of the as-prepared PAA/PSS-MWNTs was stable, and no phase separation involving nanotube aggregation was observed—not even after 2 weeks. The conductivities of PSS-MWNTs, PAA-MWNTs, and PAA/PSS-MWNTs films formed by drop-casting on glass were calculated from sheet resistance measured using the four-point probe method (Keithley 2400 source meter). The film thickness was measured with a surface profiler (Alpha Step 500, TENCOR). The PAA/PSS, the pristine MWNTs, PAA/PSS-MWNTs, and UV-cross-linked PAA/PSS-MWNTs, spin-coated on gold substrates, were characterized by ultraviolet photoemission spectroscopy (UPS) (Escalab 220IXL) using He I emission of 21.2 eV to measure the films' work functions. During the UPS measurements, a −5.0 eV bias was applied to improve the transmission of low kinetic energy electrons and ensure the determination of the energy of the low kinetic energy edge.

OFETs with bottom-contact configurations, where the source/drain electrodes are built before depositing the semiconductor layer, were fabricated on heavily doped silicon wafers covered by thermally grown 300 nm thick silicon dioxide layers. The substrates were modified with hexamethyldisilazane (HMDS) after rinsing with acetone and cleaning with a UV-ozone cleaner, GCS-1700 (AHTECH LTS (Korea)), for 20 min. ADC photo-cross-linker was added to the PAA/PSS-MWNT solution at 25 mg/mL. The PAA/PSS-MWNT solutions were spin-coated on these substrates, cross-linked by 254 nm UV light with a shadow mask for 4 min, and developed in water to remove un-cross-linked material. The channel length (L) and width (W) of patterned source/drain electrodes were 100 and 1000 μm, respectively. A solution of TIPS-PEN in toluene (1 wt %) was then dropped onto the patterned substrates and dried under ambient conditions. The electrical characteristics of the OFETs were measured in air using Keithley 2400 and 236 source/measure units.

3. RESULTS AND DISCUSSION

Figure 2 shows the conductivities of PAA-MWNT and PSS-MWNT films at different ratios of MWNTs and PAA or PSS. Upon varying the ratios of PAA to MWNTs and of PSS to MWNTs from 2:1 to 4:1 and then to 8:1, we observed a decrease in conductivity caused by an excess of PAA and

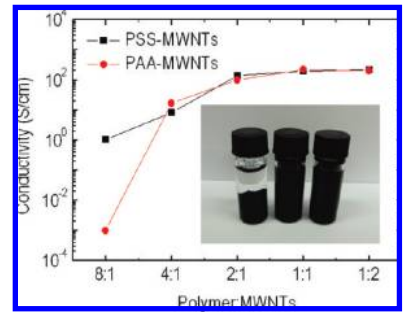

FIGURE 2. Electrical conductivities of PSS-MWNT and PAA-MWNT films as a function of the MWNT:PSS and MWNT:PAA ratios, respectively. The inset at the bottom shows 4 mL vials containing untreated MWNTs (left), PSS-MWNT (middle), and PAA-MWNT (right).

Table 1. pH, Acid Ionization Constants (K_a), and Ionization Fractions f_i of $A^-/(A+A^-)$ for PSS and PAA

	PSS (0.1 M)	PAA (0.1 M)
pH	1.60	2.98
K_a	8.4×10^{-3}	1.1×10^{-5}
f_i	0.25	0.01

PSS. At PAA:MWNT and PSS:MWNT ratios of 1:1, the conductivities became saturated at 2.0×10^2 and 2.1×10^2 S/cm, respectively. However, at a ratio of 1:2, there was insufficient PAA and PSS to disperse the nanotubes, and aggregates of MWNTs were observed. Therefore, we concluded that 1:1 ratios for MWNT:PAA and MWNT:PSS were optimal in our case. Solutions with 1:1 ratios for MWNT:PAA and MWNT:PSS were homogenously dispersed in water, even after 2 weeks. However, without PAA and PSS, nanotube aggregates in water precipitated to the bottom of the vial, as shown in the inset of Figure 2.

Although PAA and PSS dispersed MWNTs with long-term dispersion stability, PAA-MWNTs and PSS-MWNTs consisted of dispersed aggregates of bundled and strongly entangled MWNTs, preventing MWNT films from having high resolution. The proportion of aggregates largely depended on the strength of the polymer surfactant, because stronger polymer surfactants break up MWNTs bundles and disentangle MWNTs into individual tubes. The strength of the polymer surfactants is determined by the ionic strength of the polymer pendant group: benzenesulfonic acid in PSS and carboxylic acid in PAA. The acid ionization constants, K_a, of PAA and PSS were measured from the pH of 0.1 M PAA or PSS in water (Table 1). The K_a values of PAA and PSS are 1.1×10^{-5} and 8.4×10^{-3}, respectively. From these values, we found that only 1% of the PAA carboxylic acid groups were deprotonated, implying that the almost completely uncharged PAA was highly coiled due to extensive intramolecular hydrogen bonding. In contrast, 25% of the PSS benzenesulfonic acid groups were ionized, resulting in an extended polymer chain due to the Coulombic repulsion of negatively charged polymer pendant groups. Thus, PAA dispersed MWNT aggregates by adsorbing to them in the form of coiled structures (29, 30). On the other hand, the extended structures of PSS easily dispersed MWNTs, broke MWNT bundles, and disentangled MWNTs to form PSS-wrapped MWNTs (25, 31). Optical microscopy shows that

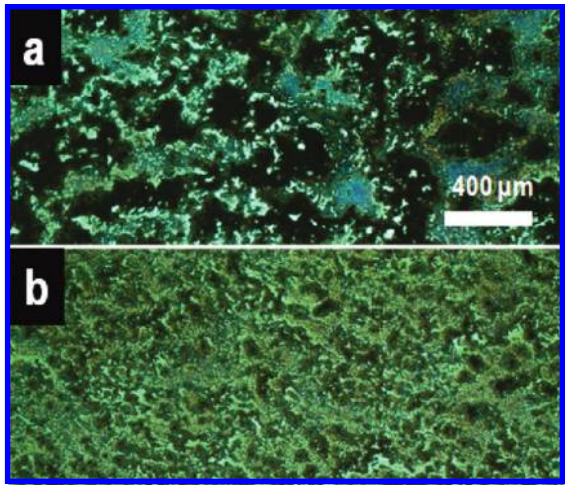

FIGURE 3. Optical microscopy images of spin-coated films of (a) PAA-MWNTs and (b) PSS-MWNTs.

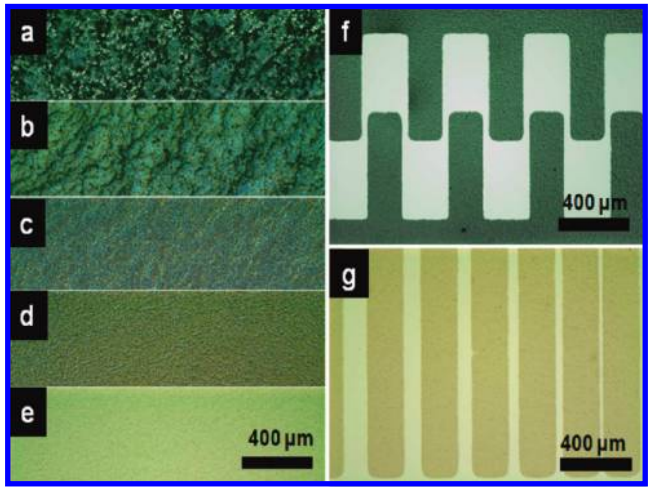

FIGURE 4. Optical microscopy images of spin-coated PAA/PSS-MWNT films obtained after centrifugation at rotor speeds of (a) 0 rpm, (b) 2500 rpm, (c) 5000 rpm, (d) 7500 rpm, and (e) 10 000 rpm and the obtained patterns of PAA/PSS-MWNT with ADC after centrifugation at rotor speeds of (f) 7500 rpm and (g) 10 000 rpm.

the films of MWNTs dispersed by PAA consisted of large aggregates that made patterning of MWNTs impossible (Figure 3a), whereas PSS-MWNTs showed much better size uniformity (Figure 3b).

Although PSS-MWNTs formed films with better uniformity, PSS-MWNTs could not be used for photopatterning because PSS is not photosensitized with ADC. To realize a photopatternable and uniform film, MWNTs were dispersed in a water solution containing a mixture of PAA/PSS, and the uniformity of the spin-coated film of PAA/PSS-MWNTs was found to be comparable to that of PSS-MWNTs, as shown in Figure 4a. A more uniform film could be obtained by removing small aggregates by centrifugation at rotor speeds of 2500, 5000, 7500, and 10 000 rpm for 20 min corresponding to 970*g*, 3900*g*, 8700*g*, and 15 500*g*, respectively. The fabricated films are shown in Figure 4b–e, respectively. Centrifugation at higher rotor speeds generated more uniform films. Speeds in excess of 7500 rpm produced sufficiently uniform films for photopatterning of space resolution of 30 μm in our laboratory (Figure 4f,g). During photo-

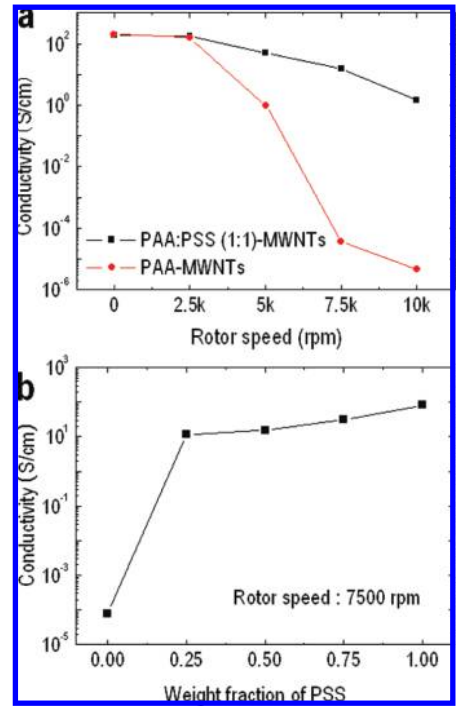

FIGURE 5. Conductivities of (a) PAA/PSS-MWNT (1:1 ratio of PAA:PSS) and PAA-MWNT after centrifugation of at different rotor speeds and (b) PAA/PSS-MWNT according to the weight fraction of PSS.

cross-linking, the conductivity only slightly decreased, by less than 10%.

One might suppose that a uniform film of PAA-MWNTs could be obtained by centrifugation of PAA-MWNTs at high rotor speed, without PSS. However, although the film of PAA-MWNTs was uniform after centrifugation, the conductivity of PAA-MWNTs was too low for use as source/drain electrodes in OFET. Figure 5a shows the conductivities of PAA-MWNTs and PAA/PSS-MWNTs as a function of rotor speed during centrifugation. The conductivity of PAA-MWNTs drastically decreased as the rotor speed increased. With speeds of 7500 rpm, the measured conductivity was below 10^{-4} S/cm, too low for use as an electrode. The conductivity of PAA/PSS-MWNT (1:1 ratio of PAA:PSS) also decreased as rotor speed increased, but the conductivity was 1.5–16 S/cm, even at speeds above 7500 rpm, which is sufficient for source/drain electrodes in OFETs. The composition of PAA and PSS in PAA/PSS-MWNTs is also important for determining conductivity. Figure 5b shows the conductivities of films drop-cast from 3 wt % PAA/PSS-MWNT with increasing PSS composition. A high composition of PSS in the PAA/PSS-MWNT increased conductivity. For photopatternable PAA/PSS-MWNTs, PAA/PSS-MWNTs should contain more than 50% of PAA. With respect to conductivity, more PSS is better, and a 1:1 ratio of PAA:PSS is optimal. Parts a and b of Figure 6 show SEM images of the pristine MWNT powder and the spin-coated film of 7500 rpm centrifuged PAA/PSS-MWNTs (1:1 ratio of PAA:PSS), respectively. The surface of the pristine MWNTs was smooth, whereas the surface of nanotubes in PAA/PSS-MWNT was rough, implying that MWNTs were covered by a polymer of PAA and PSS.

In addition to conductivity and photopatternability, the work function of materials is important for source/drain

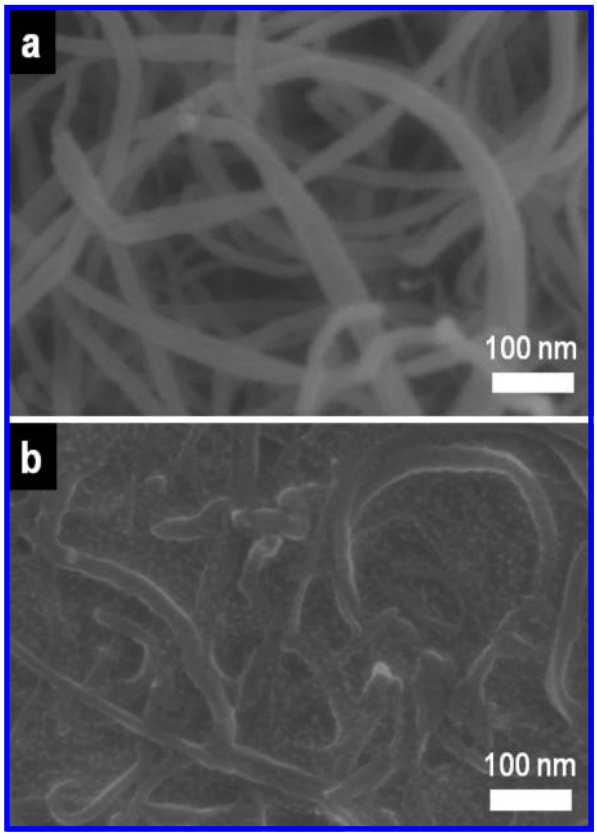

FIGURE 6. SEM images of (a) the pristine MWNTs powder and (b) a spin-coated film of PAA/PSS-MWNTs obtained after centrifugation at a rotor speed of 7500 rpm.

Table 2. Work Functions (eV) of MWNTs, PAA/PSS-Coated Gold, PAA/PSS-MWNTs, UV-Cross-Linked PAA/PSS-MWNTs, and Gold

	MWNTs	PAA/PSS-coated Au	PAA/PSS-MWNTs	UV-cross-linked PAA/PSS-MWNTs	Au
work function	4.47	4.36	4.46	4.76	5.01

electrodes in OFETs. For p-type organic semiconductors such as TIPS-PEN having an ionization energy of 5.3 eV (32), a higher work function is desirable for achieving ohmic contact between the electrode and organic semiconductor. The work function of MWNTs was measured to be 4.47 eV (Table 2) by UPS (Figure 7), consistent with previous results (33). The work function of PAA/PSS-MWNTs (4.46 eV), determined by subtracting the width of the spectrum from the source energy (21.2 eV) (34), was almost the same as that for the pristine MWNTs and similar to that of PAA/PSS-coated gold (4.36 eV). Because the value was different from the work functions of PSS-MWNTs (4.83 eV) and PAA-MWNTs (4.70 eV) (12), the work function of PAA/PSS-MWNTs did not originate from PAA-MWNT and PSS-MWNT. Instead, a complex of PSS- and PAA-covered MWNTs was likely present with randomly oriented functional groups, similar to the case for PAA/PSS-coated gold. When PAA/PSS-MWNTs were photo-cross-linked with ADC, the low work function increased to 4.76 eV, which is desirable for source/drain electrodes in p-type OFETs. The 254 nm UV light not only activates dichromate to cross-link the polymer but also

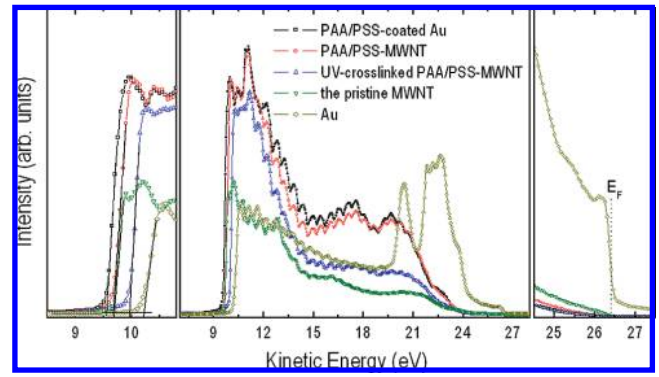

FIGURE 7. (middle) Full UP spectra of PAA/PSS-coated gold, MWNTs, PAA/PSS-MWNTs, UV-cross-linked PAA/PSS-MWNTs, and gold. (left) Close-up of the cutoff electron region to determine the work function. (right) Close-up of the Fermi edge photoemission region.

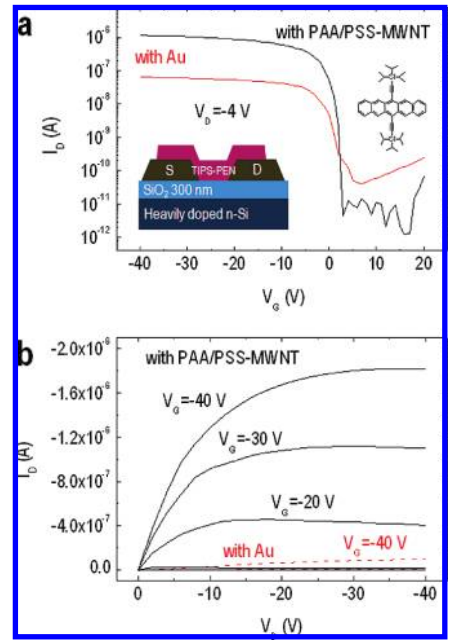

FIGURE 8. (a) I_D-V_G transfer curves in the linear regime (drain voltage $V_D = -4$ V) for TIPS-PEN OFETs containing source/drain electrodes composed of PAA/PSS-MWNTs and gold. The inset shows the OFET structure. (b) I_D-V_D output curves of both devices.

produces radicals in the polymer chains. The radicals react with oxygen in air, producing polar groups normal to the surface, such as carboxylic groups and hydroxyl groups (35). Ago et al. showed that the negative dipoles of those polar groups, oriented away from the tubes, increased the work functions of MWNTs (33). Similarly, the polar groups of PAA/PSS-MWNTs increased the work functions by 0.3 eV.

Typical drain current–gate voltage transfer curves for TIPS-PEN OFETs, fabricated using PAA/PSS-MWNT source/drain electrodes photopatterned by adding ADC photo-cross-linker, are shown in Figure 8a. The carrier mobility was calculated in the linear regime from the slope of the drain current as a function of gate voltage. This was done by fitting the data to the following equation: $I_D = (WC_i/L)\mu(V_G - V_{th})V_D$, where I_D is the drain current, μ is the carrier mobility, V_{th} is the threshold voltage, and V_D is the drain voltage (namely, -4 V) (36). The measured capacitance, C_i, was 10 nF/cm^2.

The field-effect mobility of the pentacene OFETs composed of photopatterned PAA/PSS-MWNT source/drain electrodes was 0.101 ± 0.034 cm^2/(V s) with an on/off ratio of 2×10^5, whereas that of the devices based on gold substrates was 0.012 ± 0.003 cm^2/(V s) with an on/off ratio of 3×10^3. The devices fabricated from nanotubes also showed ohmic contact behavior (Figure 8b), implying negligible contact resistance between the PAA/PSS-MWNTs and TIPS-PEN.

Although the work function of PAA/PSS-MWNTs was 0.25 eV lower than that of gold, the field-effect mobility was much higher than the field-effect mobility of OFET with gold. The higher mobility can come from morphological change of TIPS-PEN and hole injection barrier between TIPS-PEN and electrode, both of which determine contact resistance between electrodes and the semiconductor. The morphological changes of polycrystalline organic semiconductors such as vacuum-deposited pentacene and spin-coated soluble oligomer on different electrode surfaces were previously observed (37−40). However, in the case of drop-casted TIPS-PEN, we observed that large crystals were formed on the both the gold and the nanocomposite source/drain electrodes via channel and did not observe distinct morphological differences of drop-casted TIPS-PEN on gold and PAA/PSS-MWNT using polarized optical microscopy, consistent with the previously published result (32). Therefore, we believe the higher mobility of OFET-contained PAA/PSS-MWNTs come from the hole injection barrier rather than the morphological difference of TIPS-PEN on both electrodes. Many researchers report that the hole injection barrier between the organic semiconductor and the electrode was determined not only by the work function of electrodes but also by whether the electrode surface was organic or metal (37, 40, 41). Despite the high work function of gold, the hole injection barrier at the interface between the organic semiconductor and gold is large due to a large vacuum level shift. The large vacuum level shift is generally known to arise from the high induced density of interface states (IDIS) generated by the strong local orbital exchange and the potential correlation between the metal and the semiconductor (42). In contrast, the vacuum level shift between the organic semiconductor and electrodes having an organic surface is small, due to a low IDIS caused by the absence of strong local orbital exchange and the potential correlation at the interface (37, 40). Thus, the hole injection barrier between the organic semiconductor and the organic electrode is generally smaller than that between the organic semiconductor and the metal. This viewpoint implies that the interface between TIPS-PEN and gold suffers from a large vacuum level shift, leading to a higher hole injection barrier, whereas the vacuum level shift between TIPS-PEN and PAA/PSS-MWNT is small, resulting in a lower hole injection barrier. Because a smaller hole injection barrier implies a smaller contact resistance, we can assume that the higher field-effect mobility of TIPS-PEN transistors composed of PAA/PSS-MWNT source/drain electrodes originates from a contact resistance lower than that of the transistors composed of gold source/drain electrodes.

4. CONCLUSIONS

We fabricated PAA/PSS-MWNT electrodes exhibiting conductivities of 1.4−210 S/cm, satisfying the conductivity requirements for use as source/drain electrodes in OFETs, although the work function was slightly lower (4.46 eV). The PAA/PSS-MWNTs became photopatternable by adding ADC, and a minimum channel size for the OFET, using the conductive composite, was 30 μm in the laboratory. Also, the work function of the PAA/PSS-MWNTs increased to 4.76 eV during photo-cross-linking. The mobility of the TIPS-PEN field-effect transistors fabricated using PAA/PSS-MWNTs as source/drain electrodes was 0.101 ± 0.034 cm^2/(V s) with an on/off ratio of 2×10^5, about 9 times higher than that of transistors fabricated using gold source/drain electrodes (0.012 ± 0.003 cm^2/(V s)).

Acknowledgment. This work was supported by a grant from the Regional Technology Innovation Program (No. RTI04-01-04) and Strategic Technology under the Ministry of Knowledge Economy (MKE), a grant (No. F0004010-2009-32) from the Information Display R&D Center, and a grant from the Knowledge Economy Frontier R&D Program funded by the Ministry of Knowledge Economy, Government of Korea.

REFERENCES AND NOTES

(1) Dimitrakopoulos, C. D.; Malenfant, P. R. L. *Adv. Mater.* **2002**, *14*, 99.
(2) Crone, B.; Dodabalapur, A.; Lin, Y.-Y.; Filas, R. W.; Bao, Z.; Laduca, A.; Sarpeshkar, R.; Katz, H. E.; Li, W. *Nature* **2000**, *403*, 521.
(3) Sirringhaus, H.; Tessler, N.; Friend, R H. *Science* **1998**, *280*, 1741.
(4) Anthony, J. E.; Brooks, J. S.; Eaton, D. L.; Parkin, S. R. *J. Am. Chem. Soc.* **2001**, *123*, 9482.
(5) Horowitz, G.; Hajlaoui, M. E.; Hajlaoui, R. *J. Appl. Phys.* **2000**, *87*, 4456.
(6) Mcculloch, I.; Heeney, M.; Bailey, C.; Genevicius, K.; Macdonald, I.; Shkunov, M.; Sparrowe, D.; Tierney, S.; Wagner, R.; Zhang, W.; Chabinyc, M. L.; Kline, R. J.; Mcgehee, M. D.; Toney, M. F. *Nat. Mater.* **2006**, *5*, 328.
(7) Lim, J. A.; Cho, J. H.; Park, Y. D.; Kim, D. H.; Hwang, M.; Cho, K. *Appl. Phys. Lett.* **2006**, *88*, 082102.
(8) Lee, K. S.; Banchet, G. B.; Gao, F.; Loo, Y.-L. *Appl. Phys. Lett.* **2005**, *86*, 074102.
(9) Takahashi, T.; Takenobu, T.; Takeya, J.; Iwasa, Y. *Appl. Phys. Lett.* **2006**, *88*, 033505.
(10) Small, W. R.; Masdarolomoor, F.; Wallace, G. G.; Panhuis, M. *J. Mater. Chem.* **2007**, *17*, 4359.
(11) Lefenfeld, M.; Blanchet, G.; Rogers, J. A. *Adv. Mater.* **2003**, *15*, 1188.
(12) Hong, K.; Nam, S.; Yang, C.; Kim, S. H.; Chung, D. S.; Yun, W. M.; Park, C. E. *Org. Electron.* **2009**, *10*, 363.
(13) Pang, S.; Tsao, H. N.; Feng, X.; Müllen, K. *Adv. Mater.* **2009**, *21*, 1.
(14) Sirringhaus, H.; Kawase, T.; Friend, R. H.; Shimoda, T.; Inbasekaran, M.; Wu, W.; Woo, E. P. *Science* **2000**, *290*, 2123.
(15) Kumar, A.; Whiteside, G. M. *Appl. Phys. Lett.* **1993**, *63*, 2002.
(16) Chou, S. Y.; Krauss, P. R.; Renstorm, P. J. *Appl. Phys. Lett.* **1996**, *67*, 3114.
(17) Bao, Z.; Feng, Y.; Dodabalapur, A.; Raju, V. R.; Lovinger, A. J. *Chem. Matter.* **1997**, *9*, 1299.
(18) Jang, Y.; Park, Y. D.; Lim, J. A.; Lee, H. S.; Lee, W. H.; Cho, K. *Appl. Phys. Lett.* **2006**, *89*, 183501.
(19) Khong, S. H.; Sivaramakrishnan, S.; Png, R.-Q.; Wong, L.-Y.; Zhou, M.; Chua, L.-L.; Ho, P. K. H. *Adv. Funct. Mater.* **2007**, *17*, 2490.
(20) Winroth, G.; Latini, G.; Credgington, D.; Wong, L.-Y.; Chua, L.-L.; Ho, P. K. H.; Cacialli, F. *Appl. Phys. Lett.* **2008**, *92*, 103308.
(21) Touwslager, F. J.; Willard, N. P.; Leeuw, D. M. *Appl. Phys. Lett.* **2002**, *81*, 4556.

(22) Jakubowska, M.; Achmatowicz, S.; Baltrušaitis, V.; Młoøniak, A.; Wyøkiewicz, I.; Zwierkowska, E. *Microelectron. Reliability* **2008**, *48*, 860.
(23) Hatton, R. A.; Miller, A. J.; Silva, S. R. P. *J. Mater. Chem.* **2008**, *18*, 1183.
(24) Ajayan, P. M.; Ebbsen, T. W. *Rep. Prog. Phys.* **1997**, *60*, 1025.
(25) O'connel, M. J.; Boul, P.; Ericson, L. M.; Huffman, C.; Wang, Y.; Haroz, E.; Kuper, C.; Tour, J.; Ausman, K. D.; Smalley, R. E. *Chem. Phys. Lett.* **2001**, *342*, 265.
(26) Liu, A.; Honma, I.; Ichihara, M.; Zhou, H. *Nanotechnology* **2006**, *17*, 2845.
(27) Kim, J.-B.; Premukumar, T.; Lee, K.; Geckeler, K. E. *Macromol. Rapid Commun.* **2007**, *28*, 276.
(28) Barichard, A.; Israëli, Y.; Rivaton, A. *J. Polym. Sci., Part A: Polym. Chem.* **2008**, *46*, 636.
(29) Tran, N. H.; Milev, A. S.; Wilson, M. A.; Bartlett, J. R.; Kannangara, G. S. K. *Surf. Interface Anal.* **2008**, *40*, 1294.
(30) Grunlan, J. C.; Liu, L.; Regev, O. *J. Colloid Interface Sci.* **2008**, *317*, 346.
(31) Kang, Y. K.; Lee, O.-S.; Deria, P.; Kim, S. H.; Park, T.-H.; Bonnel, D. A.; Saven, J. G.; Therien, M. J. *Nano Lett.* **2009**, *9*, 1414.
(32) Hong, J.-P.; Park, A.-Y.; Lee, S.; Kang, J.; Shin, N.; Yoon, D. Y. *Appl. Phys. Lett.* **2008**, *92*, 143311.
(33) Ago, H.; Kugler, T.; Cacialli, F.; Salaneck, W. R.; Shaffer, M. S. P.; Windle, A. H.; Friend, R. H. *J. Phys. Chem. B* **1999**, *103*, 8116.
(34) Cahen, D.; Kahn, A. *Adv. Mater.* **2003**, *15*, 271.
(35) Onyiriuka, E. C. *J. Appl. Polym. Sci.* **1993**, *47*, 2187.
(36) Sze, S. *Semiconductor Devices: Physics and Technology*, 2nd ed.; Wiley: New York, 1981.
(37) Hong, K.; Lee, J. W.; Yang, S. Y.; Shin, K.; Jeon, H.; Kim, S. H.; Yang, C.; Park, C. E. *Org. Electron.* **2008**, *9*, 21.
(38) Kymissis, I.; Dimitrakopoulos, C. D.; Purushothaman, S. *IEEE Trans. Electron. Dev.* **2001**, *48*, 1060.
(39) Gundlach, D. J.; Royer, J. E.; Park, S. K.; Subramanian, S.; Jurchescu, O. D.; Hamadani, B. H.; Moad, A. J.; Kline, R. J.; Teague, L. C.; Kirillov, O.; Richter, C. A.; Kushmerick, J. G.; Richter, L. J.; Parkin, S. R.; Jackson, T. N.; Anthony, J. E. *Nat. Mater.* **2008**, *9*, 216.
(40) Hong, K.; Yang, S. Y.; Yang, C.; Kim, S. H.; Choi, D.; Park, C. E. *Org. Electron.* **2008**, *9*, 864.
(41) Wan, A.; Hwang, J.; Amy, F.; Kahn, A. *Org. Electron.* **2005**, *6*, 47.
(42) Vazquez, H.; Oszwaldowski, R.; Pou, P.; Ortega, J.; Perez, R.; Flores, F.; Kahn, A. *Europhys. Lett.* **2004**, *65*, 802.

AM900483Y